

University of Windsor

Scholarship at UWindsor

Chemistry and Biochemistry Publications

Department of Chemistry and Biochemistry

7-1-2020

The structures of polyunsaturated lipid bilayers by joint refinement of neutron and X-ray scattering data

Drew Marquardt
University of Windsor

Frederick A. Heberle
The University of Tennessee, Knoxville

Jianjun Pan
University of South Florida, Tampa

Xiaolin Cheng
The Ohio State University

Georg Pabst
Karl-Franzens-Universität Graz

See next page for additional authors

Follow this and additional works at: <https://scholar.uwindsor.ca/chemistrybiochemistrypub>

 Part of the [Biochemistry, Biophysics, and Structural Biology Commons](#), and the [Chemistry Commons](#)

Recommended Citation

Marquardt, Drew; Heberle, Frederick A.; Pan, Jianjun; Cheng, Xiaolin; Pabst, Georg; Harroun, Thad A.; Kučerka, Norbert; and Katsaras, John. (2020). The structures of polyunsaturated lipid bilayers by joint refinement of neutron and X-ray scattering data. *Chemistry and Physics of Lipids*, 229.
<https://scholar.uwindsor.ca/chemistrybiochemistrypub/149>

This Article is brought to you for free and open access by the Department of Chemistry and Biochemistry at Scholarship at UWindsor. It has been accepted for inclusion in Chemistry and Biochemistry Publications by an authorized administrator of Scholarship at UWindsor. For more information, please contact scholarship@uwindsor.ca.

Authors

Drew Marquardt, Frederick A. Heberle, Jianjun Pan, Xiaolin Cheng, Georg Pabst, Thad A. Harroun, Norbert Kučerka, and John Katsaras

The structures of polyunsaturated lipid bilayers by joint refinement of neutron and X-ray scattering data

Drew Marquardt^{a,b*}, Frederick A. Heberle^c, Jianjun Pan^d, Xiaolin Cheng^e, Georg Pabst^f, Thad A. Harroun^g, Norbert Kučerka^h, John Katsaras^{gij*}

^a*Department of Chemistry and Biochemistry, University of Windsor, Windsor, ON, Canada*

^b*Department of Physics, University of Windsor, Windsor, ON, Canada*

^c*Department of Chemistry, University of Tennessee, Knoxville, TN, 37996, USA*

^d*Department of Physics, University of South Florida, Tampa, FL, USA*

^e*Division of Medicinal Chemistry and Pharmacognosy, The Ohio State University, Columbus, OH, USA*

^f*University of Graz, Institute of Molecular Biosciences, Biophysics Division, 8010 Graz, Austria*

^g*Department of Physics, Brock University, St. Catharines, ON, Canada*

^h*Joint Institute for Nuclear Research, Frank Laboratory of Neutron Physics, Dubna, Russia and Department of Physical Chemistry of Drugs, Faculty of Pharmacy, Comenius University in Bratislava, Slovakia*

ⁱ*The Bredesen Center, University of Tennessee, Knoxville, TN, USA*

^j*Shull Wollan Center, Oak Ridge National Laboratory, Oak Ridge, TN, USA*

^k*Large Scale Structures Group, Neutron Sciences Directorate, Oak Ridge National Laboratory, Oak Ridge, TN, USA*

^k*Department of Physics and Astronomy, University of Tennessee, Knoxville, TN, USA*

Abstract

We present the detailed structural analysis of polyunsaturated fatty acid-containing phospholipids namely, 1-palmitoyl-2-docosahexaenoyl-*sn*-glycero-3-phosphocholine (PDPC) and 1-stearoyl-2-docosahexaenoyl-*sn*-glycero-3-phosphocholine (SDPC). A newly developed molecular dynamics (MD) simulation parsing scheme for lipids containing fatty acids with multiple double bonds was implemented into the scattering density profile (SDP) model to simultaneously refine differently contrasted neutron and X-ray scattering data. SDP analyses of scattering data at 30 °C yielded lipid areas of 71.1 Å² and 70.4 Å² for PDPC and SDPC bilayers, respectively, and a model free analysis of PDPC at 30 °C resulted in a lipid area of 72 Å². In addition to bilayer structural parameters, using area-constrained MD simulations we determined the area compressibility modulus, K_A , to be 246.4 mN/m, a value similar to other neutral phospholipids.

Keywords: polyunsaturated fatty acids, neutron scattering, X-ray scattering, MD simulations

1. Introduction

Phospholipids that contain polyunsaturated fatty acids (PUFAs) are a special class of lipids that constitute a biologically influential group of biomolecules essential for normal growth and development. [1] Recently, PUFA-containing phospholipids have attracted increased attention because they have been shown to be essential for a range of cellular functions [2] and for their structural and functional roles in membranes. [3] PUFAs are generally classified as *omega-3* or *omega-6* fatty acids, depending on the location of the double bond in relation to the acyl chain's terminal methyl group (i.e., *omega-3* has its last double bond located three atoms from the terminal methyl group). The dietary consumption of *omega-3* fatty acids is known to alleviate chronic health conditions including hypertension, diabetes, and arthritis [4, 5], while a diet rich in *omega-6* fatty acids is linked to increased blood viscosity, vasospasm, and vasoconstriction. [6] However, there is increasing evidence that both PUFAs are needed for maintaining good health [7] and an imbalance results in diseases such as diabetes. [5]

PUFAs associated with phospholipids exhibit increased dynamics compared to their saturated analogues. For example, the low energy barrier for rotation about C-C single bonds between olefinic and aliphatic carbons in PUFAs allows for sub-nanosecond conformational transitions, resulting in a much higher degree of chain disorder, which increases the interaction probability between PUFAs and the lipid headgroup. [8] In the case of docosahexaenoic acid (DHA; 22:6) containing lipids, it has been shown that DHA explores its entire conformational space in ~ 50 ns. [9] The high degree of PUFA chain disorder also results in thinner bilayers. An example is diarachidonoyl PC (DAPC; di20:4PC), which has an acyl chain thickness comparable to 1,2-dilauroyl-sn-glycero-3-phosphocholine (DLPC; di12:0PC), even though DAPC has eight more methines per hydrocarbon chain. [10, 11] However, a more telling example of PUFA chain disorder is given by their segmental order parameters (S_{CD}). Both simulation [12] and experimental results [13, 14] show reduced S_{CD} values ($S_{CD} < 0.05$) along the length of DHA chains in SDPC bilayers as a result of increased

28 mobility associated with their double bonds. Moreover, mixed chain PUFA PCs, such as 1-
29 palmitoyl-2-arachidonoyl-*sn*-glycero-3-phosphocholine (PAPC; 16:0-20:4PC) and 1-stearoyl-
30 2-docosahexaenoyl-*sn*-glycero-3-phosphocholine (SDPC; 18:0-22:6PC), have been reported to
31 form thinner bilayers with larger areas per lipid, compared to bilayers whose lipids contain
32 either a saturated or mono-unsaturated fatty acid chain in their *sn*-2 position. In addition
33 to their high mobility, PUFAs are susceptible to reactive oxygen species. Their vulnerability
34 to oxidation creates unique biological problems, both structurally and in terms of biological
35 availability. Structurally, PUFA oxidation products can alter the physical properties of a
36 bilayer, which can ultimately lead to the malfunction of membrane associated proteins.

37 Although not common, PUFA-containing phospholipid simulations do exist. However,
38 it appears that in some cases the existing force fields result in physically unrealistic values.
39 For example, Klauda et al. reported a headgroup-headgroup spacing (D_{HH}) for DAPC [15]
40 that is similar to the D_{HH} of POPC (36 Å), [16] but much larger than the experimen-
41 tally determined value. [10, 17] Inconsistencies between experiment and simulations thus
42 pose significant problems when trying to accurately explain the physical behavior of PUFA
43 containing phospholipids.

44 Here, we present a scattering density profile (SDP) model for lipids with PUFAs, namely
45 the mixed chain lipids 1-palmitoyl-2-docosahexaenoyl-*sn*-glycero-3-phosphocholine (PDPC;
46 16:0-22:6PC) and 1-stearoyl-2-docosahexaenoyl-*sn*-glycero-3-phosphocholine (SDPC; 18:0-
47 22:6PC). Combining small angle X-ray scattering (SAXS), small angle neutron scattering
48 (SANS), and molecular dynamics (MD) simulations we determined their bilayer structures
49 with a high degree of accuracy and unprecedented spatial resolution.

50 **2. Materials and Methods**

51 *2.1. Materials*

52 Synthetic 1-palmitoyl-2-docosahexaenoyl-*sn*-glycero-3-phosphocholine (PDPC) and 1-stearoyl-
53 2-docosahexaenoyl-*sn*-glycero-3-phosphocholine (SDPC) were purchased from Avanti Polar
54 (Alabaster, AL) lipids as chloroform solutions and used as received. Ultrapure H₂O was
55 obtained from a High-Q purification system (Wilmette, IL), and 99.9% D₂O was purchased
56 from Cambridge Isotopes (Andover, MA).

57 *2.2. Vesicle preparation*

58 Large unilamellar vesicles (LUVs) were prepared using previously established proce-
59 dures. [16, 18] In short, PDPC films were prepared by transferring the desired volumes
60 of stock lipid solutions to glass vials (Hamilton USA, Reno, NV) and then evaporating the
61 organic solvent using a combination of Ar gas and gentle heating, followed by drying in
62 vacuo for no less than 4 hours. Samples were then hydrated with 100% D₂O for SANS mea-
63 surements, or ultrapure H₂O for SAXS measurements, using a series of 7 freeze-thaw-vortex
64 cycles. The lipid dispersions were extruded using an Avanti mini-extruder with a 50 nm di-
65 ameter pore size polycarbonate filter. The SANS sample was then divided into three aliquots
66 and diluted to the desired external contrast condition (100, 75 and 50% D₂O) using an ap-
67 propriate amount of H₂O. The lipid concentration used for SAXS and SANS measurements
68 was ~ 12 mg/ml. To minimize lipid oxidation, all sample manipulations were performed in a
69 Techni-Dome 360° Glove Box Chamber under an Ar atmosphere Oxygen was measured with
70 an Oxy-Sen oxygen monitor (Alpha Omega Instruments, Cumberland, R.I.) and maintained
71 below 2% for all sample manipulations. Aliquots of the PUFA samples were taken before and
72 after SANS measurements to evaluate oxidative damage by UV/Vis spectroscopy. UV/Vis
73 experiments were conducted with an Ocean Optics USB4000 CCD array detector coupled
74 to an RF deuterium source with a tungsten halogen bulb (Mississauga, Canada) using the
75 procedure described by Marquardt et al. [10]

76 *2.3. Density measurements*

77 Lipid dispersions for volume measurements were prepared by hydrating ~ 25 mg of PDPC
78 or SDPC with ~ 1.5 g of degassed ultrapure H₂O, followed by gentle sonication at room
79 temperature until the dispersion was uniformly “milky”. Care was taken to avoid exposure
80 of the sample to oxygen, thus sample manipulations were carried out in an Ar atmosphere
81 (O₂ < 2%). The temperature dependent densities of water (ρ_w) and of the lipid dispersions
82 (ρ_s) were determined by a temperature-controlled Anton-Paar DMA5000 (Graz, Austria)
83 vibrating tube densitometer. The lipid volume (V_L), at a given temperature, was calculated
84 as previously described [19, 20, 21]

$$V_L = \frac{MW_L}{N_A \rho_s} \left[1 + \frac{m_w}{m_s} \left(1 - \frac{\rho_s}{\rho_w} \right) \right] \quad (1)$$

85 where MW_L is the molecular weight of the lipid, N_A is Avogadro's number, and m_L and
 86 m_W are the masses of the lipid and water, respectively.

87 *2.4. Small-angle neutron and X-ray scattering*

88 X-ray data were taken at the Cornell High Energy Synchrotron Source (CHESS) G-1
 89 station. 1.18 Å wavelength X-ray photons were detected using a 1024 × 1024 pixel array
 90 FLICAM charge-coupled device (CCD) with 71 μm linear dimension pixels. Samples were
 91 taken up in 1 mm quartz capillaries placed in a homemade temperature-controlled, mul-
 92 tiple position sample holder. Neutron scattering experiments were performed at the High
 93 Flux Isotope Reactor (HFIR) CG-3 Bio-SANS instrument located at Oak Ridge National
 94 Laboratory (ORNL). ULV suspensions were loaded into 2 mm path-length quartz banjo
 95 cells (Hellma USA, Plainview, NY), sealed under an Ar atmosphere, and mounted in a
 96 temperature-controlled cell holder. Data were taken at a sample-to-detector distance (SDD)
 97 of 1.7 meters using 6 Å wavelength neutrons ($\Delta\lambda/\lambda = 0.15$), resulting in a total scattering
 98 vector of $0.02 < q < 0.3 \text{ \AA}^{-1}$. Scattered neutrons were collected using a 192 × 192 pixel
 99 two-dimensional (1 m × 1 m) ^3He position-sensitive detector (ORDELA, Inc., Oak Ridge,
 100 TN). Two-dimensional data were reduced into a one-dimensional scattering intensity (I) vs
 101 the scattering vector (q) plot using ORNL's MANTID software. [22]

102 *2.5. Molecular dynamics simulations*

103 The CHARMM-GUI Membrane Builder [23] was used to generate coordinates for a PDPC
 104 bilayer containing a total of 200 lipids. Lipid hydrogen atoms were explicitly included (all-
 105 atom model), including 6962 water molecules. MD simulations were performed using the
 106 NAMD 2.9 [24] and CHARMM 36 lipid force fields. [25] Periodic boundary conditions were
 107 applied and for each system, energy was minimized using the conjugated gradient algorithm
 108 for 5000 steps, followed by 2 ns of equilibration in a constant particle number, pressure,
 109 and temperature (NPT) ensemble. Equilibrium was determined by monitoring the system's
 110 area per lipid and its root-mean-square deviation (RMSD). In all simulations, the van der

111 Waals (vdW) interactions were truncated via a potential-based switching function used by
112 X-PLOR. Starting from a switching distance of 8 Å, the vdW force was brought smoothly to
113 zero at the cut-off distance of 12 Å. Electrostatic interactions were treated using the particle-
114 mesh Ewald (PME) method with a 1.0 Å grid spacing. [26] The r-RESPA multiple-time-step
115 method [27] was employed with a 2 fs time step for bonded, and 2 and 4 fs time steps
116 for short-range nonbonded and long-range electrostatic interactions, respectively. Bonds
117 between hydrogens and other atoms were constrained using the SHAKE algorithm. [28]

118 We first simulated the PDPC bilayer using the NPT ensemble for 80 ns. Langevin
119 dynamics were used to maintain a constant temperature of 303 K, while the Nose-Hoover
120 Langevin-piston algorithm [29, 30] was used to maintain a constant pressure of 1 bar. The
121 z-axis was allowed to expand and contract independently of the x-y plane (semi-isotropic
122 pressure coupling). The resulting equilibrated lipid area was 63.5 Å². This simulation
123 was then used to guide the development of an SDP model for the joint analysis of the
124 SAXS and SANS data that resulted in an area per lipid of 70.2 Å². An additional set of
125 7 constant particle number, area, normal pressure, and temperature (NAPnT) simulations
126 was performed, where the average area per lipid was constrained to 64, 66, 68, 70, 72, 74,
127 and 76 Å², while the z-axis was allowed to expand and contract in order to maintain a
128 constant Pn. Starting configurations for these simulations were selected snapshots from the
129 NPT trajectory with lipid areas set close to their target values. The production run length
130 for each of these simulations was between 96 and 128 ns, of which only the final 50 ns of
131 each trajectory were used for data analysis. For each of the area-constrained simulations
132 the surface tension, γ , was calculated from the difference between the normal and lateral
133 components of the pressure tensor. [31, 32] The lateral area compressibility modulus, K_A , was
134 given by $K_A = \partial\gamma/\partial(\ln A)$. [33] All simulations were conducted on the Hopper supercomputer
135 located at the National Energy Research Scientific Computing Center (NERSC).

136 3. Results and Discussion

137 **Sample Integrity** PUFA's are extremely sensitive to oxidative damage. Thus, to deter-
138 mine if any oxidative damage occurred over the course of a given measurement, we performed
139 UV/Vis measurements. The majority of naturally occurring carbon-based free radicals are

140 formed from the alkyl and allylic carbons in the lipid acyl chains. Allylic carbon radicals
 141 quickly isomerize, conjugating the double bonds in PUFAs, and produces the electron- π sys-
 142 tem that absorbs UV light. After SANS experimentation, small amounts of oxidized lipids
 143 were detected as a small increase in absorbance around 250 nm (Fig. 1, red curve), com-
 144 pared to a fresh lipid preparation (Fig. 1, blue curve). However, when comparing samples
 145 that underwent experimentation to those exposed intentionally to air (Fig. 1, yellow and
 146 red curves, respectively), the amount of oxidative damage incurred by the SANS samples
 147 was negligible. Moreover, successive frames of SAXS data did not show any signs of sample
 148 degradation.

149 **Insight from Area Constrained MD Simulations** Simulations were performed using
 150 lipid areas ranging from 64.0 to 76.0 \AA^2 , generating a series of neutron and X-ray form
 151 factors for each system. Bilayer form factors were generated by computing the number
 152 density distribution of each atom from the simulation trajectories. [34] Electron density and
 153 neutron scattering length density profiles were calculated by summing the product of the
 154 number density of each atom with its number of electrons or neutron scattering length,
 155 respectively. The corresponding simulated X-ray and neutron scattering form factors were
 156 calculated from the Fourier transform of the solvent-subtracted ED or NSLD profile, as
 157 was done previously. [25, 35, 36, 37] The quality of the model-free analysis compares the
 158 calculated form factors with those from experiment, where the agreement was quantified by
 159 a reduced χ^2 defined as:

$$\chi^2 = \frac{1}{N_q - 1} \sum_{i=1}^N \left(\frac{|F_s(q_i)| - k \times |F_e(q_i)|}{k \times \Delta F_e(q_i)} \right)^2, \quad (2)$$

160 where N_q is the number of experimental q-values (data points), F_s and F_e are the simu-
 161 lated and experimental form factors, respectively, ΔF_e is the experimental uncertainty, and
 162 k is a scaling factor used to minimize χ^2 .

163 Figure 2 displays the reduced neutron, X-ray, and overall χ^2 as a function of simulated
 164 area per lipid for PDPC at 30°C measured at three different SANS contrasts (i.e., 100, 75
 165 and 50% D₂O) and one SAXS contrast. Both the neutron and the overall χ^2 values are
 166 at a minimum for an area per lipid of 72.0 \AA^2 , whereas the reduced X-ray χ^2 decreases
 167 monotonically as the area per lipid increases. Figure 3 shows the model-free comparison

168 between experimental and simulated form factors for the PDPC bilayer with an area per
169 lipid constrained to 72.0 \AA^2 . Although the neutron data are in good agreement, this is not
170 the case for the X-ray form factors, especially at the minimum position near 0.3 \AA^{-1} that
171 relates to the bilayer thickness. Since the minimum position of the simulated X-ray form
172 factor occurs at a smaller scattering vector q than the experimental X-ray form factor, we
173 can surmise that the simulated bilayer lipid area of 72 \AA^2 is too small. This observation
174 partially explains why the X-ray reduced χ^2 becomes smaller when the simulation lipid area
175 increases (and the bilayer thickness decreases). Collectively, Figs. 2 and 3 suggest that the
176 simulated bilayer at $A = 72 \text{ \AA}^2$ can qualitatively reproduce experimental scattering data
177 (especially neutron form factors), whereas further tuning of the force field is required to
178 better match the X-ray data and the area per lipid predicted by our SDP model, something
179 that has been noted previously and highlights unresolved issues with simulations [38]. It
180 should be pointed out that the fit to the neutron data leads to A directly (considering only
181 the total molecular volume obtained densitometrically), whereas the X-ray data are sensitive
182 to the values of D_{HH} and D_{H1} from the simulation. The simulations presented here provide
183 nevertheless an important basis for the SDP model described below.

184 **Lateral bilayer area compressibility** Similar to the work of Waheed and Edholm [39],
185 we used a series of MD simulations to determine the area compressibility modulus from the
186 surface tension at several different lipid areas. Figure 4 shows the calculated γ of PDPC
187 bilayers at different lipid areas. A linear fit to the data yields an area compressibility modulus
188 of 246.4 mN/m , a value consistent with K_A values of other PC lipids [40, 33], and in good
189 agreement with previously determined K_A values for PUFAs [40].

190 **SDP Model for PDPC and SDPC** Previous SDP models for phospholipid containing
191 mono-unsaturated fatty chains divided the acyl chains into terminal methyl (CH_3), methine
192 (CH), and methylene (CH_2) groups. [41, 42, 16, 36] Here, we adopted a similar parsing
193 scheme for PDPC, except for the methine groups. Due to the increased number of olefinic
194 carbons in docosahexaenoyl chains, our modified parsing scheme groups three CH groups
195 into one component, represented by a Gaussian function, as shown in Figure 4 (CHa and
196 CHb for a total of two components). For the headgroup, we used the same parsing scheme
197 as previous SDP PC models. [41, 42, 16], with one exception. Previous SDP analyses of PC

198 lipids used a V_{HL} of 331 \AA^3 , compared to the 320 \AA^3 we used here and which we form the
 199 area-constrained PDPC bilayer simulations ($A = 72.0 \text{ \AA}^2$, please see above). This value for
 200 V_{HL} is also consistent with previous experimental headgroup volume measurements [43] and
 201 using V_{HL} values of 331 \AA^3 and 320 \AA^3 results in PUFA areas per lipid that differ by ~ 0.5
 202 \AA^2 , a difference that is considerably smaller than the experimental uncertainty ($\sim 1.5 \text{ \AA}^2$)
 203 that we determined for the final PDPC area. Similar to our previous SDP model-based
 204 analyses [41, 37, 16, 35, 36], certain parameters were constrained to enhance the robustness
 205 of the fits to the data. Specifically, in addition to V_{HL} , the experimentally determined V_L
 206 was fixed and soft constraints were applied to a group of parameters, whereby any deviation
 207 from the target values determined from MD simulations resulted in a quadratic penalty to
 208 the overall χ^2 – soft-constrained parameters are denoted by an asterisk (*). Finally, the
 209 distance between two CH components (i.e., $z_{CHb} - z_{CHa}$) was constrained. In the absence
 210 of such constraint the CHs tended to move in opposite directions, resulting in unphysical
 211 distances between the two moieties.

212 **Joint SANS/SAXS analysis** An SDP example used to jointly refine PDPC bilayer
 213 SANS and SAXS data at 30°C is shown in Figure 5. The volume probability of each compo-
 214 nent (Fig. 5E) is scaled by the component electron number and neutron scattering length,
 215 respectively, to generate the ED (Fig. 5C) and NSLD (Fig. 5D) profiles. The X-ray (Fig.
 216 5B) and neutron (Fig. 5A) form factors are the Fourier transform of the total ED and NSLD
 217 profiles (after subtracting for bulk water), respectively. Results of these fits are presented
 218 in Table 1 for PDPC at 20°C , 30°C , and 40°C , as well as for SDPC at 30°C . Table 1 also
 219 compares structural parameters obtained from the area-constrained MD simulations.

220 An important parameter commonly used to describe lipid bilayer structures is A , which
 221 is determined through a combination of lipid volumetric measurements and the bilayer thick-
 222 ness. Specifically, A is related to the overall bilayer thickness, D_B , through the relationship
 223 $A = 2V_L/D_B$, where V_L is the total lipid volume and D_B is the Luzzati bilayer thickness,
 224 i.e., the Gibbs dividing surface found between the bilayer and water [44]. Alternatively, A
 225 can be calculated based on the hydrocarbon chain thickness D_C , which corresponds to the
 226 interface between polar/nonpolar parts, i.e., $A = V_{HC}/D_C$. Other structural parameters
 227 listed in Table 1 are the headgroup-to-headgroup distance, D_{HH} , and the distance between

228 the glycerol and phosphate groups, D_{H1} . Finally, σ_{HC} is the width of the error function
 229 describing the total hydrocarbon chain region, z_{CHi} and σ_{CHi} are the Gaussian center and
 230 width of the components (CHa, CHb, CH3, G1, G2 and G3). r_{CH} and r_{CH3} are the volume
 231 ratios of V_{CH}/V_{CH2} and V_{CH3}/V_{CH2} , where V_{CH} , V_{CH2} , and V_{CH3} refer to the average vol-
 232 umes of the CH, CH2 and CH3 components, respectively, and r_{G1} and r_{G2} are the volume
 233 fractions, respectively, of the G1 and G2 components with respect to the total headgroup
 234 volume.

235 SDP analysis of PDPC bilayers at 30 °C resulted in an area per lipid of 71.1 Å², in good
 236 agreement with the 72.0 Å² determined by MD simulations (Table 1). This difference is
 237 mainly due to the following: (i) D_B , which in conjunction with V_L determines the area per
 238 lipid, is more accurately obtained from SANS data; and (ii) the reduced SANS χ^2 value is
 239 smallest at 72.0 Å² (i.e., the simulation of neutron form factors at 72.0 Å² agree best with the
 240 experimental data). The discrepancy between MD data and the X-ray form factor (Fig. 3) is
 241 reflected by the difference in D_{HH} values between the simulated bilayer and the SDP model
 242 prediction. The larger D_{HH} value from the simulated bilayer indicates that simulations with
 243 smaller D_{HH} will agree better with the experimental X-ray form factor. (Note that D_{HH} is
 244 defined by the maxima in the ED profile.)

245 Compared to previously reported SDP data for mixed chain lipids, the area per lipid
 246 value for PDPC at 30 °C is ~ 7 Å² larger than that of POPC lipids (i.e., 64.3 Å²). [16] Con-
 247 sistent with the lipid area result, the hydrocarbon chain thickness, $2D_C$, of PDPC bilayers
 248 is ~ 1 Å smaller than that of POPC bilayers. [16] The values for A and $2D_C$ for PDPC are
 249 consistent with a disordered *sn*-2 PUFA chain. Not surprisingly, a monotonically increasing
 250 area per lipid with increasing temperature observed for PDPC is consistent with what has
 251 been reported previously. [16] Similarly, area per lipid of SDPC is ~ 4.9 Å² larger than its
 252 mono-unsaturated analogue SOPC (i.e., 65.5 Å²) [16], along with its associated invariance
 253 of $2D_C$. Interestingly, A for SDPC is identical to PDPC, within experimental error. That is,
 254 exchanging the palmitoyl fatty acid chain with stearoyl does not affect lipid packing, as this
 255 bilayer property is dominated by the presence of the disordered docosahexaenoyl acyl chain
 256 at the *sn*-2 position. Unfortunately, a direct comparison of PDPC and SDPC with their fully
 257 saturated analogues is not possible at these temperatures as di-palmitoyl PC and di-stearoyl

258 PC only exist in the gel phase at the reported temperatures. The other thickness param-
259 eters associated with PDPC and SDPC are notably smaller than their mono-unsaturated
260 analogues; i.e., D_B and D_{HH} are ~ 2 Å and ~ 4 Å smaller, respectively. This observation
261 is consistent with the notion of the PUFA chain “snorkeling” up to the lipid headgroup
262 region. The PUFA chains reside at the lipid-water interface an appreciable amount of time,
263 thereby necessitating that the headgroups remain in its tilted orientation in order to shield
264 the PUFA (umbrella model) [45] from the aqueous solvent, similar to what has previously
265 been seen with POPC and SOPC bilayers. [46] It is worth noting that the dependency of area
266 per lipid on acyl chain length is sensitive to the unsaturation and position of double bonds,
267 mismatch in the unsaturation and length of the two chains, and likely to other structural
268 characteristics of lipids. [47, 48] For example, the area decrease with increasing chain length
269 was reported for di-saturated PCs, while the elongation of saturated chain in the case of
270 saturated/mono-unsaturated lipids resulted in the area increase.[11]

271 Subtle but important differences in lipid bilayer structure induced by the presence of a
272 PUFA chain, rather than a mono-unsaturated chain, can have profound biological impli-
273 cations. The transverse structure of a membrane has implications associated with integral
274 protein stability, enzyme activation, and modulating charge–membrane interactions. [49]
275 These results are yet another example of the importance of lipid diversity and how different
276 lipid species affect the transmembrane structure.

277 4. Summary

278 We combined MD simulations with differently contrasted SANS and SAXS data to de-
279 termine the structure of the PUFA containing phospholipids PDPC and SDPC with a high
280 degree of structural detail. Simulations guided a model-based analysis of the experimental
281 data that resulted in an area per lipid of 71.1 Å² for PDPC at 30 °C. This result was sup-
282 ported by model free evaluation of PDPC bilayers, where simulations with different fixed
283 areas were directly compared to experimental data and which yielded an area per PDPC of
284 72.0 Å². Future work will make use of the current SDP model and strategy to determine the
285 bilayer structures for other commonly studied PUFA containing phospholipids. Importantly,
286 the discrepancy between the different contrast scattering and simulations data, considering

287 that the neutron and X-ray data sets were obtained using the same LUVs (prepared using
288 the sample method), emphasizes the need for the further refinement of the MD simulation
289 force fields.

290 **Acknowledgments**

291 SANS data were collected at the Bio-SANS instrument located at the High Flux Iso-
292 tope Reactor, a DOE Office of Science User Facility operated by the Oak Ridge National
293 Laboratory. The authors also wish to acknowledge personnel support from the Center for
294 Structural Molecular Biology. J.K. is supported through the Scientific User Facilities Divi-
295 sion of the Department of Energy (DOE) Office of Science, sponsored by the Basic Energy
296 Science (BES) Program, DOE Office of Science, under Contract No. DEAC05-00OR22725.
297 F.A.H acknowledges support from National Science Foundation grant No. MCB-1817929.
298 D.M. acknowledges the support of the Natural Sciences and Engineering Research Council
299 of Canada (NSERC), [funding reference number RGPIN-2018-04841].

300 **References**

- 301 [1] D. L. O'Connor, R. Hall, D. Adamkin, N. Auestad, M. Castillo, W. E. Connor, S. L.
302 Connor, K. Fitzgerald, S. Groh-Wargo, E. E. Hartmann, J. Jacobs, J. Janowsky, A. Lu-
303 cas, D. Margeson, P. Mena, M. Neuringer, M. Nesin, L. Singer, T. Stephenson, J. Szabo,
304 V. Zemon, Growth and Development in Preterm Infants Fed Long-Chain Polyunsat-
305 urated Fatty Acids: A Prospective, Randomized Controlled Trial, *PEDIATRICS* 108
306 (2001) 359–371. doi:10.1542/peds.108.2.359.
- 307 [2] J. Hamilton, R. Greiner, N. Salem, H.-Y. Kim, n-3 Fatty acid deficiency decreases
308 phosphatidylserine accumulation selectively in neuronal tissues, *Lipids* 35 (2000) 863–
309 869. doi:10.1007/S11745-000-0595-x.
- 310 [3] A. Catalá, Lipid peroxidation modifies the picture of membranes from the “Fluid
311 Mosaic Model” to the “Lipid Whisker Model”, *Biochimie* 94 (2012) 101–109.
312 doi:10.1016/j.biochi.2011.09.025.

- 313 [4] W. Stillwell, S. R. Wassall, Docosahexaenoic acid: membrane properties of a unique
314 fatty acid, *Chemistry and Physics of Lipids* 126 (2003) 1–27. doi:10.1016/S0009-
315 3084(03)00101-4.
- 316 [5] A. P. Simopoulos, Human Requirement for N-3 Polyunsaturated Fatty Acids, *Poultry*
317 *Science* 79 (2000) 961–970. doi:10.1093/ps/79.7.961.
- 318 [6] A. P. Simopoulos, Essential fatty acids in health and chronic disease, *The American*
319 *Journal of Clinical Nutrition* 70 (1999) 560s–569s. doi:10.1093/ajcn/70.3.560s.
- 320 [7] A. P. Simopoulos, Omega-6/Omega-3 Essential Fatty Acid Ratio and Chronic Diseases,
321 *Food Reviews International* 20 (2004) 77–90. doi:10.1081/FRI-120028831.
- 322 [8] N. V. Eldho, S. E. Feller, S. Tristram-Nagle, I. V. Polozov, K. Gawrisch, Polyunsatu-
323 rated Docosahexaenoic vs Docosapentaenoic Acid Differences in Lipid Matrix Properties
324 from the Loss of One Double Bond, *Journal of the American Chemical Society* 125
325 (2003) 6409–6421. doi:10.1021/ja029029o.
- 326 [9] O. Soubias, K. Gawrisch, Docosahexaenoyl Chains Isomerize on the Sub-Nanosecond
327 Time Scale, *Journal of the American Chemical Society* 129 (2007) 6678–6679.
328 doi:10.1021/ja068856c.
- 329 [10] D. Marquardt, J. A. Williams, N. Kučerka, J. Atkinson, S. R. Wassall, J. Katsaras,
330 T. A. Harroun, Tocopherol Activity Correlates with Its Location in a Membrane: A
331 New Perspective on the Antioxidant Vitamin E, *Journal of the American Chemical*
332 *Society* 135 (2013) 7523–7533. doi:10.1021/ja312665r.
- 333 [11] T. A. Harroun, J. Katsaras, S. R. Wassall, Cholesterol Hydroxyl Group Is Found To
334 Reside in the Center of a Polyunsaturated Lipid Membrane, *Biochemistry* 45 (2006)
335 1227–1233. doi:10.1021/bi0520840.
- 336 [12] X. Leng, J. J. Kinnun, D. Marquardt, M. Ghefli, N. Kučerka, J. Katsaras, J. Atkinson,
337 T. A. Harroun, S. E. Feller, S. R. Wassall, α -Tocopherol Is Well Designed to Protect
338 Polyunsaturated Phospholipids: MD Simulations, *Biophysical Journal* 109 (2015) 1608–
339 1618. doi:10.1016/j.bpj.2015.08.032.

- 340 [13] S. E. Feller, K. Gawrisch, A. D. MacKerell, Polyunsaturated Fatty Acids in Lipid Bi-
341 layers: Intrinsic and Environmental Contributions to Their Unique Physical Properties,
342 Journal of the American Chemical Society 124 (2002) 318–326. doi:10.1021/ja0118340.
- 343 [14] K. Gawrisch, N. V. Eldho, L. L. Holte, The structure of DHA in phospholipid mem-
344 branes, Lipids 38 (2003) 445–452. doi:10.1007/s11745-003-1082-0.
- 345 [15] J. B. Klauda, V. Monje, T. Kim, W. Im, Improving the CHARMM Force Field for
346 Polyunsaturated Fatty Acid Chains, The Journal of Physical Chemistry B 116 (2012)
347 9424–9431. doi:10.1021/jp304056p.
- 348 [16] N. Kučerka, M.-P. Nieh, J. Katsaras, Fluid phase lipid areas and bilayer
349 thicknesses of commonly used phosphatidylcholines as a function of temperature,
350 Biochimica et Biophysica Acta (BBA) - Biomembranes 1808 (2011) 2761–2771.
351 doi:10.1016/j.bbamem.2011.07.022.
- 352 [17] T. A. Harroun, J. Katsaras, S. R. Wassall, Cholesterol Is Found To Reside in the
353 Center of a Polyunsaturated Lipid Membrane, Biochemistry 47 (2008) 7090–7096.
354 doi:10.1021/bi800123b.
- 355 [18] F. A. Heberle, R. S. Petruzielo, J. Pan, P. Drazba, N. Kučerka, R. F. Standaert,
356 G. W. Feigenson, J. Katsaras, Bilayer Thickness Mismatch Controls Domain Size in
357 Model Membranes, Journal of the American Chemical Society 135 (2013) 6853–6859.
358 doi:10.1021/ja3113615.
- 359 [19] O. Kratky, H. Leopold, H. Stabinger, The determination of the partial specific volume
360 of proteins by the mechanical oscillator technique., Methods in enzymology 27 (1973)
361 98–110. URL: <http://www.ncbi.nlm.nih.gov/pubmed/4797943>. doi:10.1016/s0076-
362 6879(73)27007-6.
- 363 [20] A. Hodzic, M. Rappolt, H. Amenitsch, P. Laggner, G. Pabst, Differential Modulation
364 of Membrane Structure and Fluctuations by Plant Sterols and Cholesterol, Biophysical
365 Journal 94 (2008) 3935–3944. doi:10.1529/biophysj.107.123224.

- 366 [21] J. Pan, F. A. Heberle, S. Tristram-Nagle, M. Szymanski, M. Koepfinger, J. Katsaras,
367 N. Kučerka, Molecular structures of fluid phase phosphatidylglycerol bilayers as de-
368 termined by small angle neutron and X-ray scattering, *Biochimica et Biophysica Acta*
369 (BBA) - Biomembranes 1818 (2012) 2135–2148. doi:10.1016/j.bbamem.2012.05.007.
- 370 [22] O. Arnold, J. Bilheux, J. Borreguero, A. Buts, S. Campbell, L. Chapon, M. Doucet,
371 N. Draper, R. Ferraz Leal, M. Gigg, V. Lynch, A. Markvardsen, D. Mikkelson,
372 R. Mikkelson, R. Miller, K. Palmen, P. Parker, G. Passos, T. Perring, P. Peterson,
373 S. Ren, M. Reuter, A. Savici, J. Taylor, R. Taylor, R. Tolchenov, W. Zhou, J. Zikovsky,
374 Mantid—Data analysis and visualization package for neutron scattering and μ SR ex-
375 periments, *Nuclear Instruments and Methods in Physics Research Section A: Ac-*
376 *celerators, Spectrometers, Detectors and Associated Equipment* 764 (2014) 156–166.
377 doi:10.1016/j.nima.2014.07.029.
- 378 [23] S. Jo, J. B. Lim, J. B. Klauda, W. Im, CHARMM-GUI Membrane Builder for Mixed
379 Bilayers and Its Application to Yeast Membranes, *Biophysical Journal* 97 (2009) 50–58.
380 doi:10.1016/j.bpj.2009.04.013.
- 381 [24] J. C. Phillips, R. Braun, W. Wang, J. Gumbart, E. Tajkhorshid, E. Villa, C. Chipot,
382 R. D. Skeel, L. Kalé, K. Schulten, Scalable molecular dynamics with NAMD, *Journal*
383 *of Computational Chemistry* 26 (2005) 1781–1802. doi:10.1002/jcc.20289.
- 384 [25] J. B. Klauda, R. M. Venable, J. A. Freites, J. W. O’Connor, D. J. Tobias, C. Mondragon-
385 Ramirez, I. Vorobyov, A. D. MacKerell, R. W. Pastor, Update of the CHARMM All-
386 Atom Additive Force Field for Lipids: Validation on Six Lipid Types, *The Journal of*
387 *Physical Chemistry B* 114 (2010) 7830–7843. doi:10.1021/jp101759q.
- 388 [26] T. Darden, D. York, L. Pedersen, Particle mesh Ewald: An $N \log(N)$ method for
389 Ewald sums in large systems, *The Journal of Chemical Physics* 98 (1993) 10089–10092.
390 doi:10.1063/1.464397.
- 391 [27] M. Tuckerman, B. J. Berne, G. J. Martyna, Reversible multiple time scale molecular
392 dynamics, *The Journal of Chemical Physics* 97 (1992) 1990–2001. doi:10.1063/1.463137.

- 393 [28] J.-P. Ryckaert, G. Ciccotti, H. J. Berendsen, Numerical integration of the cartesian
394 equations of motion of a system with constraints: molecular dynamics of n-alkanes,
395 Journal of Computational Physics 23 (1977) 327–341. doi:10.1016/0021-9991(77)90098-
396 5.
- 397 [29] G. J. Martyna, M. L. Klein, M. Tuckerman, Nosé–Hoover chains: The canonical ensem-
398 ble via continuous dynamics, The Journal of Chemical Physics 97 (1992) 2635–2643.
399 doi:10.1063/1.463940.
- 400 [30] S. E. Feller, Y. Zhang, R. W. Pastor, B. R. Brooks, Constant pressure molecular
401 dynamics simulation: The Langevin piston method, The Journal of Chemical Physics
402 103 (1995) 4613–4621. doi:10.1063/1.470648.
- 403 [31] J. Sonne, F. Y. Hansen, G. H. Peters, Methodological problems in pressure profile
404 calculations for lipid bilayers, The Journal of Chemical Physics 122 (2005) 124903.
405 doi:10.1063/1.1862624.
- 406 [32] O. Berger, O. Edholm, F. Jähnig, Molecular dynamics simulations of a fluid bilayer of
407 dipalmitoylphosphatidylcholine at full hydration, constant pressure, and constant tem-
408 perature, Biophysical Journal 72 (1997) 2002–2013. doi:10.1016/S0006-3495(97)78845-3.
- 409 [33] A. R. Braun, J. N. Sachs, J. F. Nagle, Comparing Simulations of Lipid Bilayers to Scat-
410 tering Data: The GROMOS 43A1-S3 Force Field, The Journal of Physical Chemistry
411 B 117 (2013) 5065–5072. doi:10.1021/jp401718k.
- 412 [34] N. Kučerka, J. Katsaras, J. F. Nagle, Comparing membrane simulations to scattering
413 experiments: introducing the SIMtoEXP software., The Journal of membrane biology
414 235 (2010) 43–50. doi:10.1007/s00232-010-9254-5.
- 415 [35] J. Pan, D. Marquardt, F. A. Heberle, N. Kučerka, J. Katsaras, Revisiting the bilayer
416 structures of fluid phase phosphatidylglycerol lipids: Accounting for exchangeable hy-
417 drogens, Biochimica et Biophysica Acta (BBA) - Biomembranes 1838 (2014) 2966–2969.
418 doi:10.1016/j.bbamem.2014.08.009.

- 419 [36] J. Pan, X. Cheng, L. Monticelli, F. A. Heberle, N. Kučerka, D. P. Tieleman, J. Katsaras,
420 The molecular structure of a phosphatidylserine bilayer determined by scattering and
421 molecular dynamics simulations, *Soft Matter* 10 (2014) 3716. doi:10.1039/c4sm00066h.
- 422 [37] N. Kučerka, B. van Oosten, J. Pan, F. A. Heberle, T. A. Harroun, J. Katsaras, *Molecular*
423 *Structures of Fluid Phosphatidylethanolamine Bilayers Obtained from Simulation-to-*
424 *Experiment Comparisons and Experimental Scattering Density Profiles*, *The Journal*
425 *of Physical Chemistry B* 119 (2015) 1947–1956. doi:10.1021/jp511159q.
- 426 [38] J. F. Nagle, *Introductory lecture: Basic quantities in model biomembranes*, *Faraday*
427 *Discuss.* 161 (2013) 11–29. doi:10.1039/C2FD20121F.
- 428 [39] Q. Waheed, O. Edholm, *Undulation Contributions to the Area Compressibil-*
429 *ity in Lipid Bilayer Simulations*, *Biophysical Journal* 97 (2009) 2754–2760.
430 doi:10.1016/j.bpj.2009.08.048.
- 431 [40] W. Rawicz, K. Olbrich, T. McIntosh, D. Needham, E. Evans, *Effect of Chain Length*
432 *and Unsaturation on Elasticity of Lipid Bilayers*, *Biophysical Journal* 79 (2000) 328–339.
433 doi:10.1016/S0006-3495(00)76295-3.
- 434 [41] N. Kučerka, J. F. Nagle, J. N. Sachs, S. E. Feller, J. Pencer, A. Jackson,
435 J. Katsaras, *Lipid Bilayer Structure Determined by the Simultaneous Analysis of*
436 *Neutron and X-Ray Scattering Data*, *Biophysical Journal* 95 (2008) 2356–2367.
437 doi:10.1529/biophysj.108.132662.
- 438 [42] N. Kučerka, J. Gallová, D. Uhríková, P. Balgavý, M. Bulacu, S.-J. Marrink, J. Katsaras,
439 *Areas of Monounsaturated Diacylphosphatidylcholines*, *Biophysical Journal* 97 (2009)
440 1926–1932. doi:10.1016/j.bpj.2009.06.050.
- 441 [43] W.-J. Sun, R. M. Suter, M. A. Knewton, C. R. Worthington, S. Tristram-Nagle,
442 R. Zhang, J. F. Nagle, *Order and disorder in fully hydrated unoriented bilayers of*
443 *gel-phase dipalmitoylphosphatidylcholine*, *Physical Review E* 49 (1994) 4665–4676.
444 doi:10.1103/PhysRevE.49.4665.

- 445 [44] J. F. Nagle, S. Tristram-Nagle, Structure of lipid bilayers, *Biochimica et Biophys-*
446 *ica Acta (BBA) - Reviews on Biomembranes* 1469 (2000) 159–195. doi:10.1016/S0304-
447 4157(00)00016-2.
- 448 [45] J. Huang, G. W. Feigenson, A Microscopic Interaction Model of Maximum Sol-
449 ubility of Cholesterol in Lipid Bilayers, *Biophysical Journal* 76 (1999) 2142–2157.
450 doi:10.1016/S0006-3495(99)77369-8.
- 451 [46] J. F. Nagle, Experimentally determined tilt and bending moduli of single-
452 component lipid bilayers, *Chemistry and Physics of Lipids* 205 (2017) 18–24.
453 doi:10.1016/j.chemphyslip.2017.04.006.
- 454 [47] H. I. Petrache, A. Salmon, M. F. Brown, Structural properties of do-
455 cosahexaenoyl phospholipid bilayers investigated by solid-state 2h nmr spec-
456 troscopy, *Journal of the American Chemical Society* 123 (2001) 12611–12622. URL:
457 <https://doi.org/10.1021/ja011745n>. doi:10.1021/ja011745n, PMID: 11741426.
- 458 [48] K. Rajamoorthi, H. I. Petrache, T. J. McIntosh, M. F. Brown, Packing and vis-
459 coelasticity of polyunsaturated -3 and -6 lipid bilayers as seen by 2h nmr and x-ray
460 diffraction, *Journal of the American Chemical Society* 127 (2005) 1576–1588. URL:
461 <https://doi.org/10.1021/ja046453b>. doi:10.1021/ja046453b, PMID: 15686391.
- 462 [49] L. B. Li, I. Vorobyov, T. W. Allen, The role of membrane thickness in charged pro-
463 tein–lipid interactions, *Biochimica et Biophysica Acta (BBA) - Biomembranes* 1818
464 (2012) 135–145. doi:10.1016/j.bbamem.2011.10.026.

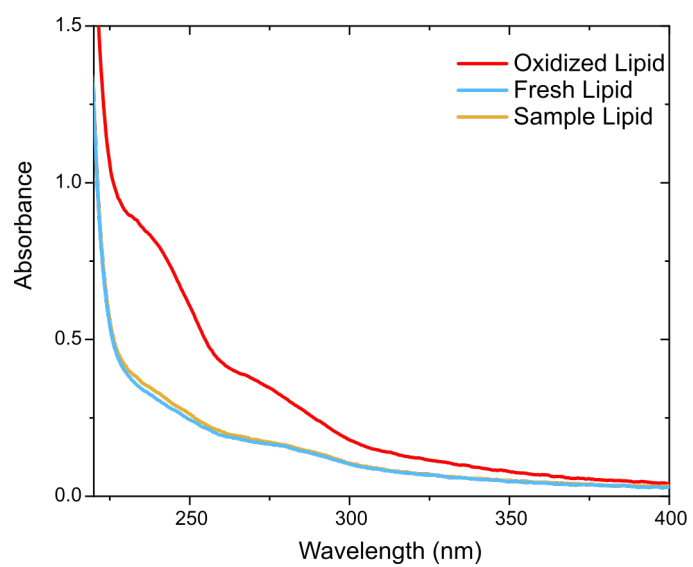


Figure 1: UV absorption spectra of SDPC bilayers composed of oxidized lipid (red line), freshly prepared lipid (blue), and a sealed sample studied by SANS approximately 12 hours after the measurement (orange line). The oxidized lipid was exposed to air for 12 hours.

Table 1: SDP Structural Data of PDPC Bilayers

	PDPC				SDPC
	SDP model	SDP model	SDP model	CHARMM	SDP model
	20°C	30°C	40°C	30°C	30°C
V_L (Å ³)	1296.6**	1306.4**	1316.1**	1312.0	1366.4**
V_{HL} (Å ³)	320.0**	320.0**	320.0**	320.0	320.0**
A (Å ²)	69.3	71.1	72.9	72.0	70.4
D_B (Å)	37.4	36.8	36.1	36.4	38.8
D_{HH} (Å)	33.2	33.0	32.2	36.8	35.2
$2D_C$ (Å)	28.2	27.8	27.3	27.5	29.7
D_{H1} (Å)	2.51	2.63	2.43	4.63	2.73
z_{G1} (Å)	15.3	14.9	14.6	15.0	16.1
σ_{G1} (Å)	2.84	2.82	2.70	2.88	2.89
z_{G2} (Å)	16.7	17.0	16.6	19.0	17.7
σ_{G2} (Å)	3.23	3.30	3.37	2.95	3.14
z_{G3} (Å)	20.2*	20.0*	19.9*	20.5	20.9*
σ_{G3} (Å)	3.45*	3.44*	3.44*	3.46	3.46*
z_{CHb} (Å)	8.6	8.00	7.8	10.1	8.0
σ_{CHb} (Å)	3.52*	3.52*	3.52*	3.50	3.51*
z_{CHa} (Å)	2.8	2.2	2.0	4.3	2.3
σ_{CHa} (Å)	4.08*	4.07*	4.07*	4.1	4.08
$z_{CHb} - z_{CHa}$ (Å)	5.8*	5.8*	5.8*	5.8	5.7*
σ_{HC} (Å)	2.84*	2.84*	2.83*	2.83	2.82*
σ_{CH3} (Å)	3.70*	3.70*	3.70*	4.20	3.88*
r_{G1}	0.45*	0.44*	0.44*	0.45	0.45*
r_{G2}	0.36*	0.36*	0.36*	0.36	0.36*
r_{CH3}	2.02*	2.02*	2.02*	1.97	2.01*
r_{CH}	0.92*	0.92*	0.92*	0.92	0.92*

Parameters are shown with their appropriate units for length (Å), area (Å²), and volume (Å³). Estimated uncertainties are $\pm 2\%$. The double asterisk (**) denotes fixed parameters, while a single asterisk (*) denotes “soft” constrained parameters, allowed to vary within limits.

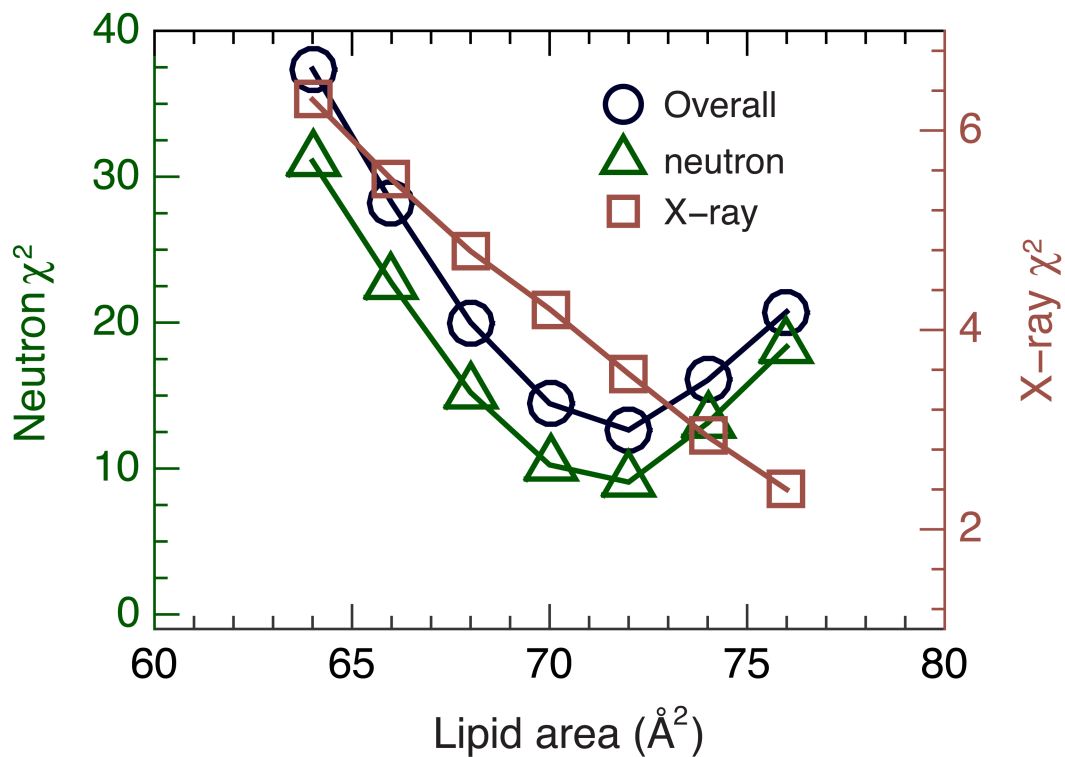


Figure 2: Model-free comparisons between experimental and simulated form factors for predetermined PDPC lipid areas. The neutron χ^2 (open triangle, left axis) was obtained by summing the squares of the neutron form factor differences at 3 D₂O contrasts weighted by their experimental uncertainties and number of data points. The X-ray χ^2 (open square, right axis) was obtained in a similar manner except that there is only one set of X-ray data. The overall χ^2 (open circle, left axis) is a combination of neutron and X-ray χ^2

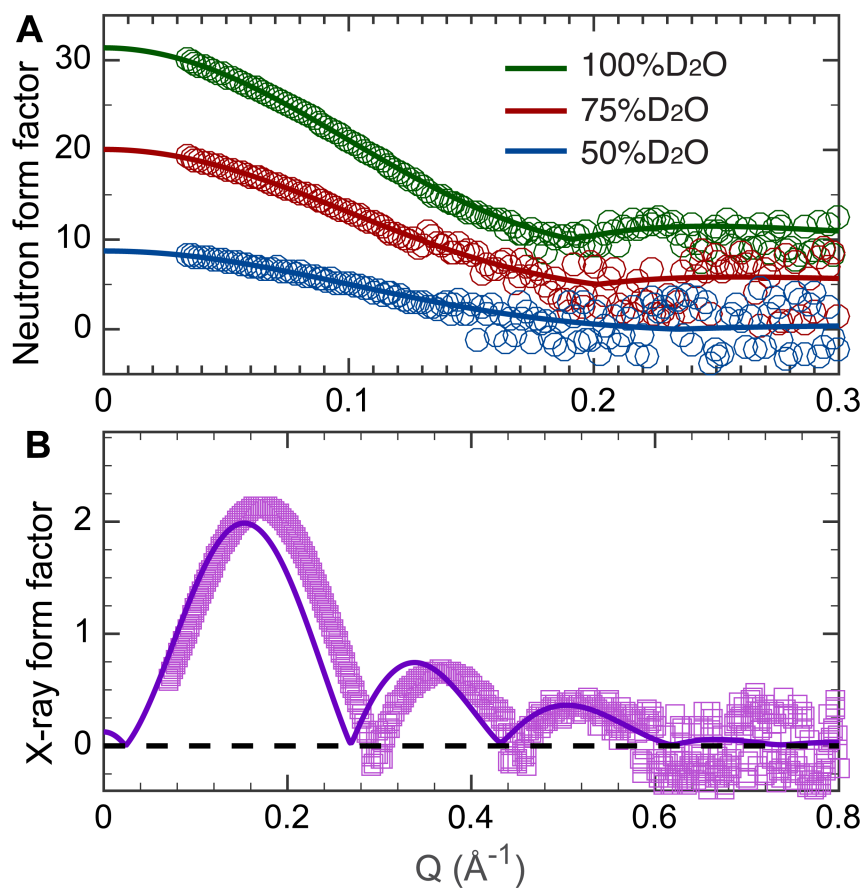


Figure 3: Model-free comparison between experimental scattering data and a simulated PDPC bilayer with an area per lipid constrained to 72.0 \AA^2 . The different contrast experimental (A) neutron and (B) X-ray form factors (symbols) are the same as those used in the SDP model analysis. The corresponding simulation form factors (solid lines) were calculated from atom number density distributions obtained from *NAPnT* simulations. Each experimental form factor was scaled by a coefficient to minimize the reduced χ^2 , after taking experimental uncertainties into account.

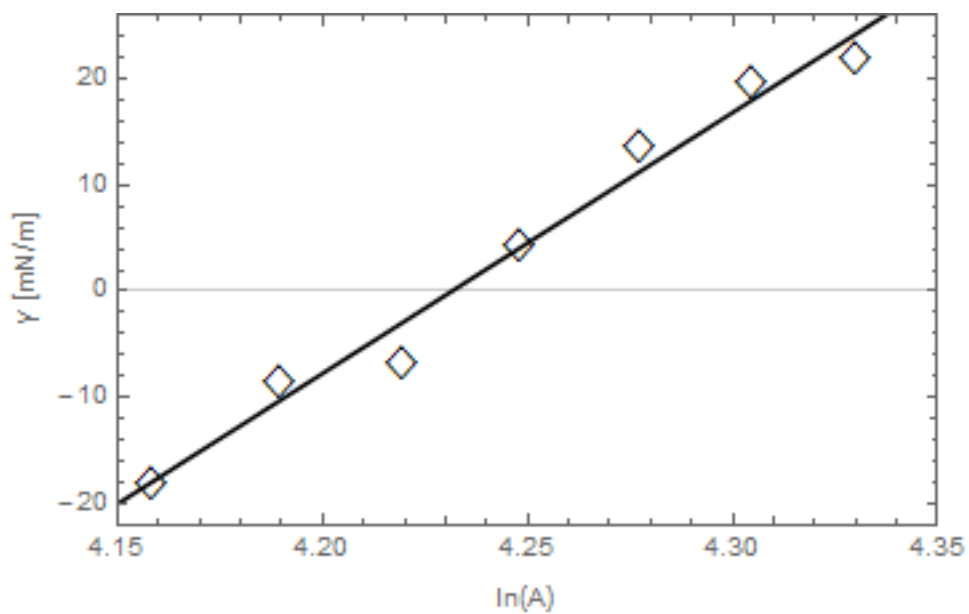


Figure 4: Lateral surface tension applied to a PDPC bilayer as a function of lipid area (A). The linear fit to the data (solid line) resulted in a calculated area compressibility modulus of $K_A = 246.4$ mN/m.

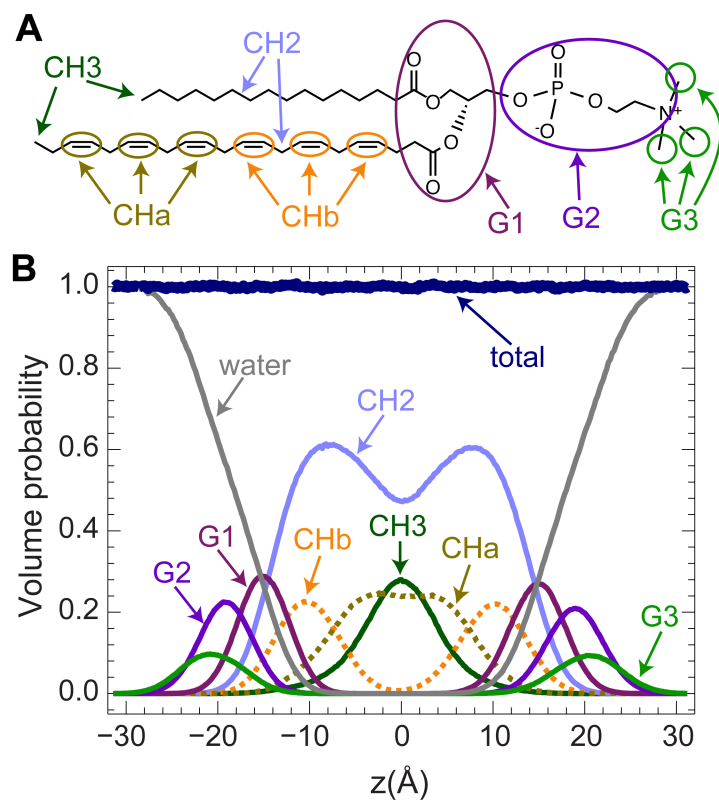


Figure 5: Parsing scheme for a PDPC bilayer based on MD simulations. A) The chemical structure of PDPC with different moieties is highlighted. B) The volume probabilities of each component based on the parsing scheme. Fatty acid chains were divided into terminal methyl (CH₃), methylene (CH₂) and methine (CH), with double bonds grouped together as CH_a and CH_b. The PC headgroup was parsed into the carbonyl-glycerol (G1), phosphate+CH₂CH₂N (G2) and the choline methyls (G3).

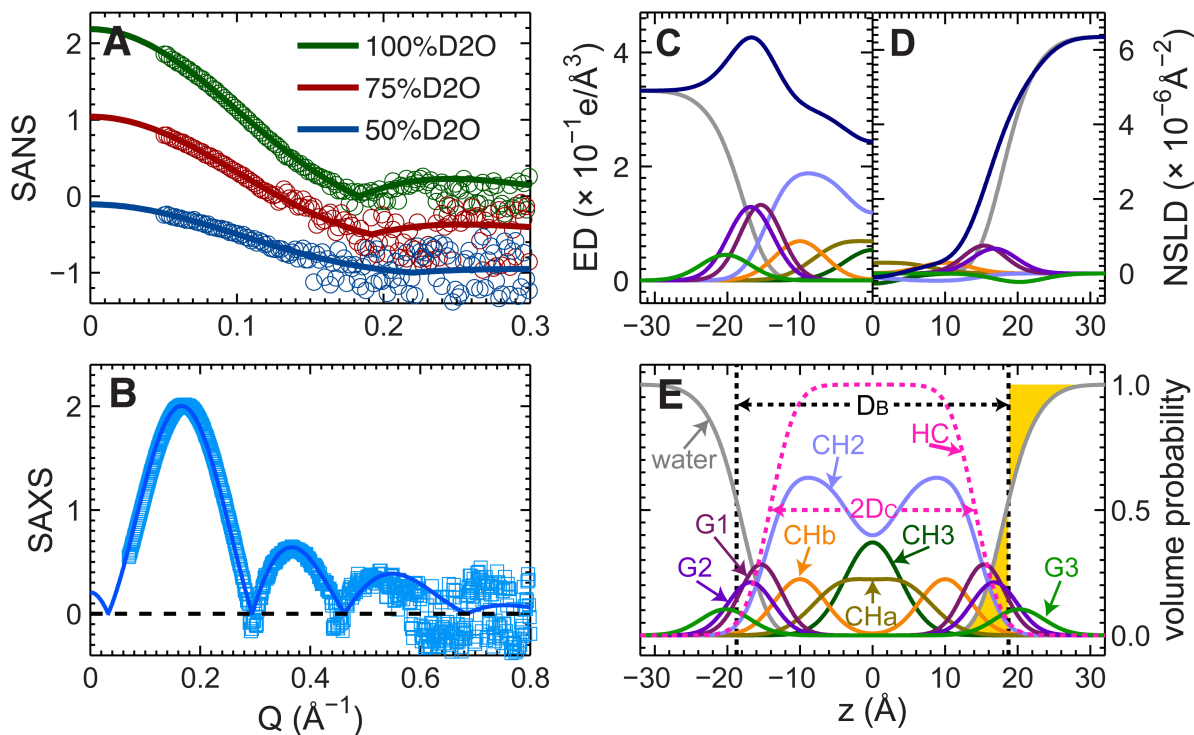


Figure 6: Fits (solid lines) to the experimental SANS (A) and SAXS (B) form factors (points) for PDPC at 30 °C using SDP. Panels on the right show the SDP model of the PDPC bilayer in real space, where the top panels show electron densities (C) and neutron scattering length densities (D) of the components making up the bilayer, including the total scattering densities (thick lines). (E) Bottom panel illustrates the volume probability distributions, where the total probability is equal to 1 at each point along the bilayer normal.